

Merging SPOT for Landscape-Ecological Studies, Applied to a Coastal Dune Environment

Tjeerd Willem Hobma

Faculty of Earth Sciences

Department of Hydrology

Free University Amsterdam

De Boelelaan 1085

1081 HV Amsterdam, The Netherlands

ABSTRACT

HOBMA, T.W., 1995. Merging SPOT for landscape-ecological studies, applied to a coastal dune environment. *Journal of Coastal Research*, 11(4), 1003-1019. Fort Lauderdale (Florida), ISSN 0749-0208.



The use of satellite remote sensing in landscape-ecological studies has been limited until now by the generally unfavourable spatial and spectral resolutions of the sensors. A concise overview is given of current and future developments in the SPOT and Landsat programs that may be of interest for coastal researchers concerned with mapping of natural vegetation and landscape elements at a sub-regional scale. A method is described in which optimum use is made of the combination of multispectral and panchromatic imagery for mapping vegetation structure in a coastal dune in the south-western delta of the Netherlands. Mean evapotranspiration rates, taken from the literature for each type of vegetation, were finally used to visualize the spatial variability of evapotranspiration and to estimate groundwater recharge within a coastal dune environment. It is demonstrated that the Radiometric Method for merging SPOT-XS and PAN can be used not only to improve rectification accuracies, to depict greater cartographic detail and to enhance spatial resolution but also to improve results of a supervised classification in a fine-grained landscape. In the future the merging procedure will be especially useful for processing multispectral and panchromatic data of SPOT5 and Landsat-7.

ADDITIONAL INDEX WORDS: *Remote sensing, coastal dune, vegetation mapping, evapotranspiration.*

INTRODUCTION

In landscape-ecological studies at regional and sub-regional scales the heterogeneity of the landscape is a central issue. Satellite remote sensing is not always a suitable technique for mapping the landscape because of the limitations of the sensors. Landsat and SPOT have been providing series of images for some years already. However, the spatial and spectral resolutions of the data often do not match the requirements (HOBMA, 1991). Developments that may be of interest for landscape-ecological studies concern the new satellites Landsat-6 and SPOT4 and-5.

Table 1 illustrates in which parts of the optical spectrum and at which spatial resolution Landsat-5 and SPOT1 and-2 have been observing the earth until today. Presently Landsat and SPOT both have different advantages for mapping vegetation, *i.e.*, a good spectral resolution (Landsat-5) and a good spatial resolution (SPOT1 and-2). Table 2 provides the supplementary or

modified technical data of Landsat-6 (launched but unfortunately missing since the end of 1993) and SPOT4 (from 1997). From looking at both tables, it follows that Landsat-6 will have a high resolution band (TM-PAN, spatial resolution 15 m) and SPOT4 will have a band in the middle-infrared (XS4, spatial resolution 20 m). Future spatial resolutions of SPOT5 will be 10 m in multispectral and even 5 m in panchromatic mode! For the time being SPOT1,-2 and-3 will be optically identical (NLR, 1993). Of less importance for this study and therefore not mentioned in the tables is the spatial resolution of the thermal band of Landsat-5 and-6 (TM6). Here the innovation consists in an increase of the spatial resolution from 120 m towards 60 m on Landsat-7 (NLR, 1993). For vegetation mapping, it is interesting that in the future Landsat-7 and SPOT4 will both be able to provide complete multispectral and panchromatic data, at increasing spatial resolutions.

The described developments will have two important consequences for research and operational use of remote sensing. First, the management

Table 1. Spectral and spatial parameters of Landsat-5 and SPOT1 and -2 in the present situation (from PRICE, 1987; NLR, 1993).

Satellite	Band	Spectral Resolution (mm)		Spatial Resolution (m)	
		Center Wave-length	Band-width	Ground Reso-lution	Pixel Size
Landsat-5	TM1	480	61	30	28.5
	TM2	570	74	30	28.5
	TM3	660	67	30	28.5
	TM4	830	127	30	28.5
	TM5	1670	209	30	28.5
	TM7	2210	235	30	28.5
	SPOT1 and -2	XS1	540	107	20
XS2		650	77	20	20
XS3		840	102	20	20
PAN		620	211	10	10

of the ever increasing amount of data is going to be one of the major challenges of the coming years. SPOT5, for example, will provide five times as much data in the future than in the present situation. Second, it is essential that efficient methods be developed in which the benefits of the improved spatial, spectral and temporal resolutions of the satellite images are optimally used. This will strongly improve and increase the application of satellite remote sensing for mapping natural vegetation and landscape elements at a sub-regional scale.

In this paper, a method is presented which combines multispectral and high resolution panchromatic data of SPOT, called merging (PRICE, 1987b). The Radiometric Method for merging (PELLEMANS *et al.*, 1993) has been applied with SPOT-XS and SPOT-PAN data. With the use of supplementary information, vegetation structure and spatial variability of evapotranspiration have been mapped in a coastal dune area in the southwestern delta of the Netherlands.

ENVIRONMENTAL PROBLEM DEFINITION

The Coastal Dune Environment

The coastal dune area De Manteling/Oranjezon comprises a series of parallel dune ridges with former wet dune slacks in between and some adjacent old estates in the south on the peninsula of Walcheren (Figure 1). The dunes of Oranjezon constitute a narrow groundwater recharge area (442 ha) with a maximum width of 1 km. Since the middle ages, the coastal dune gradually ex-

Table 2. Spectral and spatial parameters of the improved sensors of Landsat-6 and SPOT-4, from end 1993 and 1997 respectively (from NLR, 1993).

Satellite	Band	Spectral Resolution (nm)		Spatial Resolution (m)	
		Center Wave-length	Band-width	Ground Resolu-tion	Pixel Size
Landsat-6	PAN	700	400	13•15	ca. 13•15
SPOT-4	XS4	1600	ca. 200	20	20

panded in north-eastern direction. Valleys in the east were connected with the open sea until 1910.

Groundwater has been extracted for public use from the dunes of Oranjezon since 1892. From 1940 until 1984, between 800.000 and 1.000.000 m³ of water per year was withdrawn. With increasing amounts of extracted groundwater, problems related to capacity and saltwater intrusion occurred frequently. From January 1984, groundwater extraction was reduced to less than 400.000 m³ per year. During the past decades, various changes in hydrology and water management have caused a significant lowering of groundwater levels in Oranjezon: *i.e.*, excessive groundwater exploitation, forestation with pine (to prevent blow-outs), increasing encroachment of shrubs and trees, changes in the position of the coastline and intensive drainage in the adjacent polder area. The resulting reduction of the water budget of the coastal dune has led to a severe decrease in nature values. Characteristic types of vegetation for wet dune slacks have dissappeared almost completely. On the strongly decalcified boggy soils, thick-thorn shrubland and dry grassland with encroachment of low woody species became dominant. In the west of Oranjezon sheltered by young birch forest, a small slack serves as a nature refuge for an endangered plant species, royal fern.

Due to the described intervention in water management, an imbalance developed in past decades; however, for some time, experiments on nature regeneration have been effected in Oranjezon (HOBMA *et al.*, 1994). The purpose of these experiments is the regeneration of wet dune slacks and their typical vegetation. Since July 1991, part of the grasslands in the west of Oranjezon have been regularly cut or grazed by cows. On August 25 1991, the date of observation by SPOT, the organic top layer was being stripped at two sites to recreate the initial conditions of a wet dune slack. In 1985, the highest central dune was dug

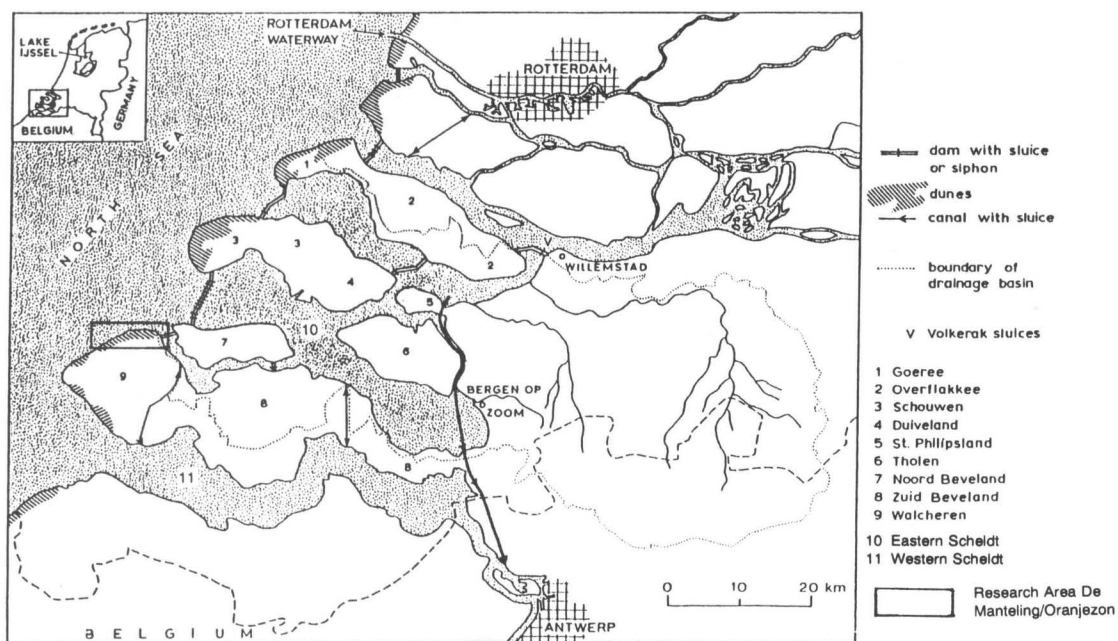


Figure 1. Situation of the coastal dune area De Manteling/Oranjezon, in the south-western delta of the Netherlands.

out down to the groundwater level to provide sand supplements on the sea wall. A small fresh water pool with swamp vegetation developed. At the end of 1992, the reconstruction works on 4 dune slacks were completed in the east of Oranjezon; groundwater extraction is now concentrated in the west of the dune area.

Environmental Research Questions

The following questions will be raised and answered in this study: (1) Does resolution enhancement by merging SPOT-XS and-PAN improve classification accuracy of a natural vegetation map of a coastal dune? (2) Is the algorithm for merging according to the Radiometric Method (PELLEMANS *et al.*, 1993) suitable for operational use? (3) How can ET-reference values for coastal dune vegetation types be used to visualize the spatial distribution of evapotranspiration in support of groundwater recharge modelling?

METHODOLOGY AND APPROACH

Methods and Data

A multispectral and a panchromatic SPOT image of the south-western delta of the Netherlands

from August 25, 1991, were selected. The specifications of the multispectral (XS) bands and the panchromatic (PAN) band are shown in Table 1. Colored aerial photographs (scale 1:18.000) were available from the north-western coast of Walcheren, taken during the summer of 1988. An old vegetation structure map (HEIDEMIJ, 1976) and a fieldmap of the vegetation structure in the extreme western part of Oranjezon (DUIN and KUST, 1991) were available too. Image processing was done on a SUN Workstation with the software packages Erdas 7.5 and Arc/Info 6.0, respectively raster and vector based.

The general approach is shown in a flowchart (Figure 2) of which the most important steps will be discussed briefly: Two images, SPOT-XS and-PAN, of a section of the Netherlands South-West Delta were geometrically referenced and corrected using a first order equation and 20 ground control points. The Nearest Neighbour algorithm was applied for resampling the multispectral image to the pixel size of the panchromatic image, 10 m. The original pixel values have been preserved. Merging SPOT-XS and-PAN was performed according to the algorithm of the Radiometric Method (PELLEMANS *et al.*, 1993). The dune

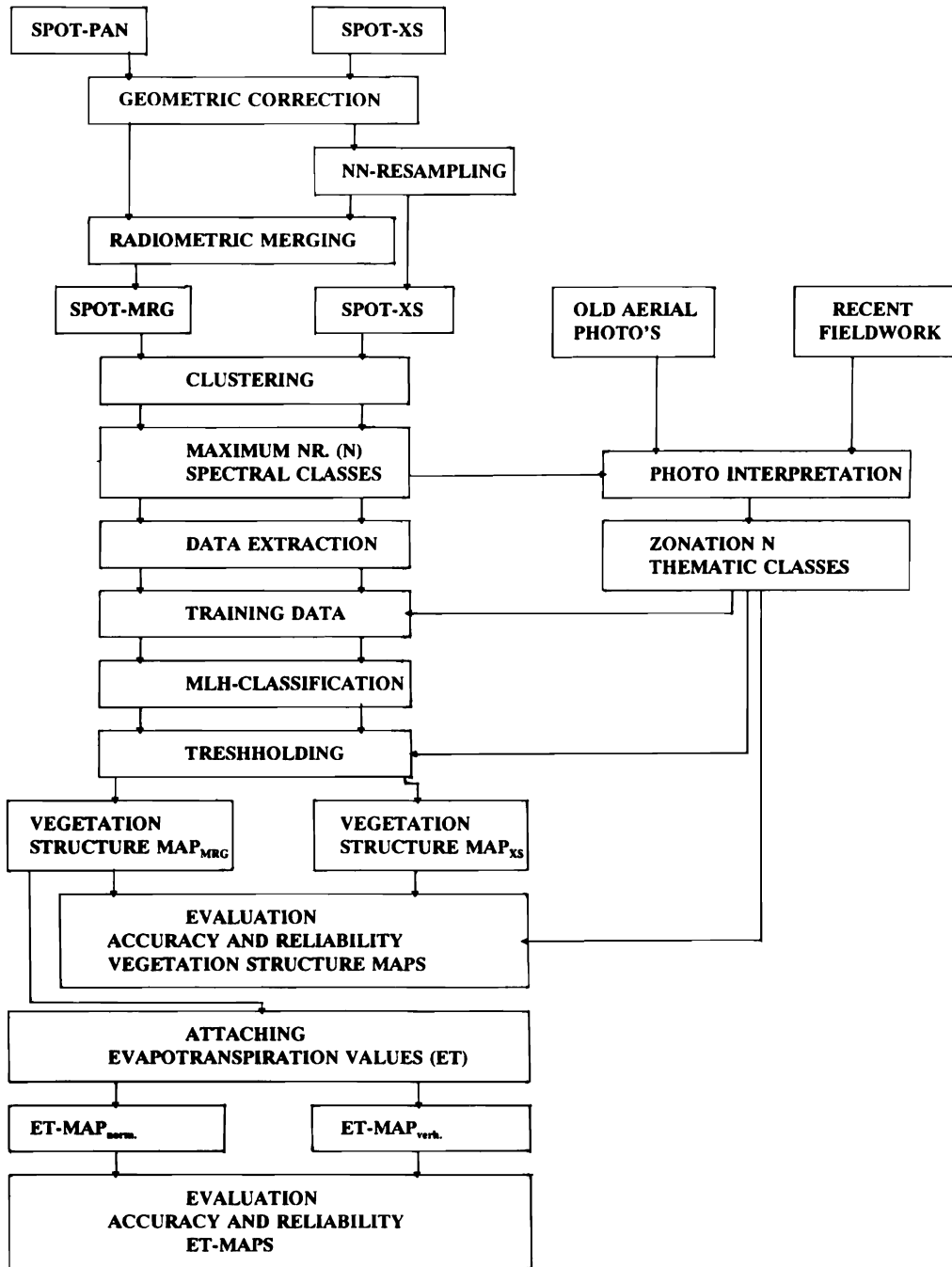


Figure 2. General approach for merging SPOT-XS and - PAN, mapping vegetation structure and evapotranspiration.

area of De Manteling/Oranjezon was extracted from the SPOT-XS and- MRG images by digitising from the screen. Using two cluster algorithms, an unsupervised classification was performed to find out how many spectral classes could be abstracted from both images. With aerial photographs and supplementary maps, a translation into 15 vegetation structure classes was made. The supplementary information was used to select training areas (29) in both images to perform a supervised classification in 14 thematic classes. Classification results based on SPOT-XS and-MRG were evaluated using a confusion matrix, aerial photographs and a recent field map. The groundwater recharge area of Oranjezon was selected from the most accurate and reliable vegetation structure map.

By attaching annual referential evapotranspiration values (ET in mm/year) to the vegetation classes (STUYFZAND, 1986, 1993; BAKKER, 1981), the spatial distribution of annual evapotranspiration in the groundwater recharge area was made. Per type of vegetation, a distinction was made between evapotranspiration at dry (normal) and wet (above normal) conditions (HOBMA *et al.*, 1995). The natural groundwater recharge was calculated as the difference between precipitation (P) and evapotranspiration (ET) in mm/year and m³/year.

The spatial distribution of annual ET in Oranjezon is reproduced in two maps with 6 ET-classes varying between < 200 and > 600 mm/year, one representing the normal and one representing the above normal situation.

Merging SPOT-XS and- PAN using the Radiometric Method

In general, merging is based on the calibration and combination of a multispectral image at spatial resolution r_m and a panchromatic image at spatial resolution r_p , where $r_m > r_p$. Here the objective of merging is to create a multispectral image at a spatial resolution equal to that of the panchromatic image, with a minimum loss of spectral information. Comparing pixel values in the multispectral image with those in the panchromatic image is not straight forward. Therefore the merging process starts with the transformation of the original multispectral image s(SPOT-XS, three bands) into a new co-ordinate system in which one of the axes represent the intensity. The integration of both types of spectral data is based on simulation of the panchro-

matic channel from the three multispectral channels, via the intensity. The intensity that is simulated by the multispectral channels is then replaced by the panchromatic channel. For this transformation, a number of solutions are available (PRICE, 1987b; CARPER *et al.*, 1990; CHAVEZ *et al.*, 1991; MUNESHIKA *et al.*, 1993; PELLEMANS *et al.*, 1993). After the inverse transformation, the resulting pixel values are not only based on the original multispectral radiances¹ but also on those in the panchromatic channel.

After merging, the pixel values are strongly related to the original multispectral pixel values. By using the absolute pixel values post-processing algorithms like vegetation indices become more useful. The original algorithm according to PELLEMANS *et al.* (1993) has been modified and applied to the SPOT imagery of August 25, 1991.

To estimate the intensity, the spectral sensitivity of the different sensors is used. In Figure 3 the spectral sensitivity curves for the instruments SPOT HRV1 and HRV2 are shown, derived from SPOT IMAGE (1988). Observed radiances in the multispectral sensors ($L_i(\lambda)$) contribute to the total radiance in the panchromatic sensor ($L_p(\lambda)$) to a lesser or larger extent. Total multispectral and panchromatic radiances can be calculated for each channel by integrating the spectral curves in Figure 3, respectively according to,

$$L_i = \int_0^{\infty} L(\lambda)H_i(\lambda) d\lambda \quad (1a)$$

$$(i = 1, 2, 3, \dots, n)$$

$$L_p = \int_0^{\infty} L(\lambda)H_p(\lambda) d\lambda \quad (1b)$$

where $H_i(\lambda)$ and $H_p(\lambda)$ represent the normalized spectral sensitivity characteristics of the multispectral sensors ($i=1,2,3, \dots, n$) and the panchromatic sensor (p).

The panchromatic radiance can be simulated (L_p^s) by linear combination of the multispectral radiances, according to,

$$L_p^s = \sum_{i=1}^n h_i \cdot L_i \quad (2)$$

The weighting factor (h_i) depends on the contribution of each multispectral channel to the

¹ Radiance is the radiation energy L in [W · m⁻² · sr⁻¹ · μm⁻¹]. L is related to the pixelvalue P, expressed as a DN [0-255], dependent on the calibration of the sensor.

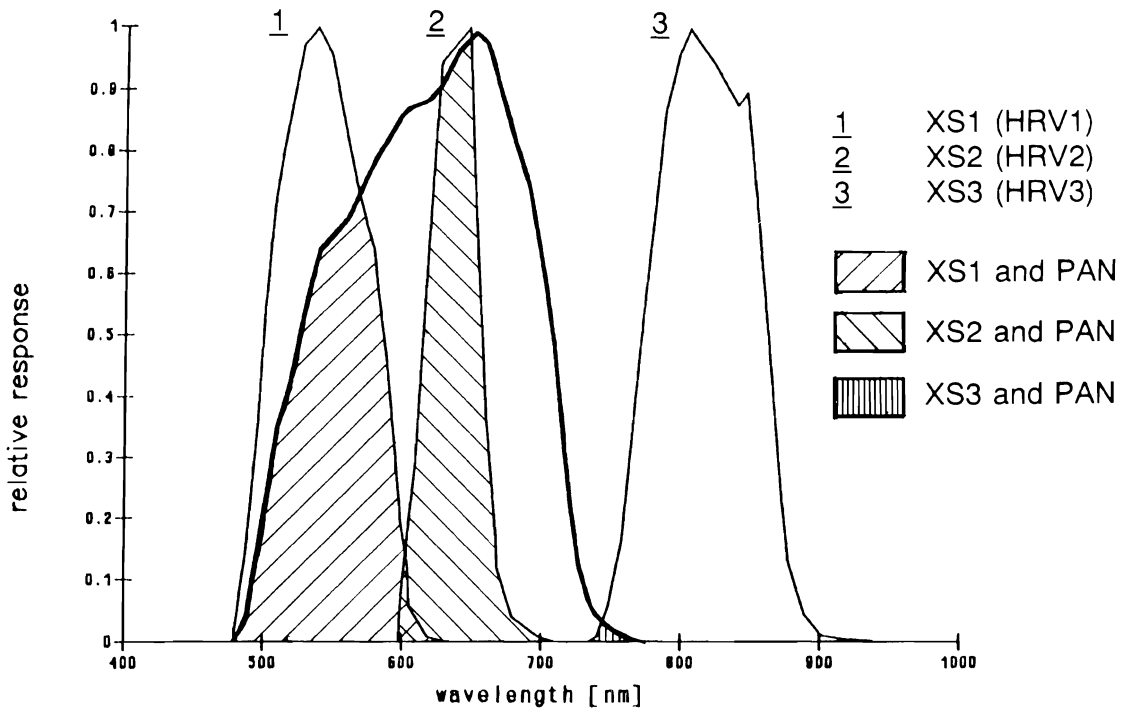


Figure 3. The spectral response curves of SPOT HRV (altered from: PELLEMANS *et al.*, 1993).

panchromatic channel. This corresponds to the overlapping area below the multispectral response curve in question and the panchromatic response curve in Figure 3. The normalized weighting factors are calculated according to,

$$h_i = \frac{\int_0^\infty H_p(\lambda)H_i(\lambda) d\lambda}{\sum_{i=1}^n \int_0^\infty H_p(\lambda)H_i(\lambda) d\lambda} \left(\sum_{i=1}^n h_i = 1 \right) \quad (3)$$

Figure 3 illustrates that for SPOT the complete multispectral contribution to the panchromatic channel comes only from Channel 1 and 2. The curve of Channel 3 doesn't show any overlap with the panchromatic curve, and although PRICE (1987b) finds a statistical correlation between the two, Channel 3 doesn't take part in this transformation. In principle, the simulated panchromatic radiance can be determined for every SPOT image in the same way by filling in Equation (2). However, since the spectral responses of the different sensors ($H_i(\lambda)$ and $H_p(\lambda)$) are not numeri-

cally available, they are idealised by assuming that the responses are uniform within each channel and zero outside. This results in weighting factors (h_i) for the multispectral channels, based on the idealised overlap with the panchromatic channel of 80, 70 and 0 nm respectively. The simulated panchromatic radiance then follows from,

$$L_p^s = \frac{80}{150}L_1 + \frac{70}{150}L_2 + \frac{0}{150}L_3 \quad (4)$$

When calculating radiances (L_i and L_p) from pixel values (P_i and P_p), one has to account for a likely different setting of the sensors of the multispectral and the panchromatic image. These settings are different for every set of SPOT images. Conversion into radiances is possible by using an absolute calibration factor (A_i and A_p) per channel². The calibration factor corrects for the difference in spectral sensitivity of the two instruments at a selected standard calibration, according to,

² $A_{i,p}$ is the absolute calibration factor for the multispectral channel i and the panchromatic channel p respectively, in $[DN \cdot W^{-1} \cdot m^2 \cdot sr \cdot \mu m]$.

Table 3. Calibration coefficients (gain numbers) of SPOT, dependent on platform (SPOT1, SPOT2), instrument (HRV1, HRV2), mode (XS1, XS2, XS3, PAN), and adjusted calibration (Low, Standard, High gain) (from SPOT Image, 1988).

Platform	Instrument	Band	Gain Number				
			Low	Stand.	High		
SPOT1	HRV1	XS1	5	6	8		
		XS2	6	7	8		
		XS3	4	5	7		
		PAN	4	4	7		
	HRV2	XS1	5	6	8		
		XS2	6	7	8		
		XS3	4	5	7		
		PAN	4	5	7		
		SPOT2	HRV1	XS1	4	6	8
				XS2	5	7	8
XS3	3			5	7		
PAN	5			7	8		
HRV2	XS1		4	6	8		
	XS2		5	7	8		
	XS3		3	5	7		
	PAN		4	6	7		

$$L_i = \frac{P_i}{A_i} \quad (i = 1, 2, 3, \dots, n) \quad (5a)$$

$$L_p = \frac{P_p}{A_p} \quad (5b)$$

In Table 3 the possible combinations of calibration coefficients (gain numbers) of SPOT are shown³, dependent on the platform (SPOT1, SPOT2), the instrument (HRV1, HRV2), the mode (PAN, XS1, XS2, XS3), and the adjusted calibration (Low, Standard, High gain). The settings during the observation on August 25, 1991⁴ (Table 4) are compared to the calibration factors (Table 3).

When during observation a non-standard calibration coefficient (Low or High gain) has been used, as is the case for the panchromatic sensor, the calibration factors for the particular setting (A_i^{mod} and A_p^{mod}) can be calculated from⁵,

$$A_i^{mod} = A_i \cdot (1.3)^{(m_0 - m)} \quad (6a)$$

$$(i = 1, 2, 3, \dots, n)$$

$$A_p^{mod} = A_p \cdot (1.3)^{(m_0 - m)} \quad (6b)$$

³ Modified according to Spot Image (1988). User's Handbook, Vol-1, (Reference Manual, pp. 3-18).

⁴ Source: Header files provided with images SPOT-XS and-PAN, 15/08/91.

⁵ Modified according to PRICE J.C. (1987a). Calibration of Satellite Radiometers and the Comparison of Vegetation Indices. *Remote Sensing of Environment*, 21, 15-27.

Table 4. SPOT instrument setting on 25/08/91.

Item	Multispectral Image	Panchromatic Image
Satellite	SPOT1	SPOT2
Mode	XS	PAN
Instrument	HRV2	HRV1
Date	1991/08/25	1991/08/25
Gain numbers	6 7 5	8
A_i	1.15808	—
A_i	1.17066	—
A_i	1.26201	—
A_p	—	1.76453

where A_i and A_p are the absolute calibration factors for the multispectral channels ($i= 1,2,3, \dots, n$) and the panchromatic channel (p), m_0 the standard calibration coefficient (Standard gain number) and m the adjusted calibration coefficient. It is easy to see that at Standard gain calibration: $m_0 - m=0$. In this case, the absolute calibration factor may be used in Equation 5.

The simulated intensity (I_1) is obtained by substitution of Equation (5b) in Equation (2). The Equations (7a and b) describe the complete transformation. It consists of the transformation from pixel values via multispectral radiances into intensities by calibration per channel and weighed linear combination of the multispectral radiances and the absolute calibration coefficients,

$$I_1 = \sum_{i=1}^n c_i P_i \quad (7a)$$

$$c_i = h_i \frac{A_p}{A_i} \quad (i = 1, 2, 3, \dots, n) \quad (7b)$$

The simulated intensity by the multispectral channels (I_1) is now replaced by the intensity of the panchromatic channel (I_p), which is set equal to the pixel value of the panchromatic channel (P_p), according to,

$$I_1 = I_p = P_p \quad (8)$$

The n multispectral channels define a n -dimensional space. The transformation into a new co-ordinate system of equation (7a), in which the intensity (I_1) is one of the axes, is to be completed with $n-1$ other normal equations. For SPOT-XS on 25/08/91: $n=3$. PELLEMANS *et al.* (1993) give one possible solution for this transformation according to the matrix notation of equation (9). By calculating inproducts, it can easily be shown that the chosen linear equations for I_2 and I_3 are perpendicular to I_1 and to each other.

Table 5. The spreadsheet containing the algorithm for merging multispectral and panchromatic SPOT imagery with the radiometric method.

Calibration and Weighting Factors for SPOT-XS and -PAN, 25/08/91						
Band	A _{i,p}	St. Gain	Mod. Gain	A _{MOD}	h _i	c _i
XS1	1.15808	6	6	1.15808	0.533	0.625
XS2	1.17066	7	7	1.17066	0.467	0.541
XS3	1.26201	5	5	1.26201	0	0
PAN	1.76453	7	8	1.35733		
r ² = 0.684		r ⁻² = 1.463 (r ² = c ₁ ² + c ₂ ²)				

Matrix of Radiometric Merging Factors for Combined Forward and Inverse Transformation				
Norm. Eq	* P _{pan}	* P _{xs1}	* P _{xs2}	* P _{xs3}
1	0.915	0.428	-0.495	0.000
2	0.792	-0.495	0.572	0.000
3	0.000	0.000	0.000	1.000

Algorithm Test for One Pixel			
Band	P _{xs,pan}	L _{xs,pan}	P _{mrq}
XS1	73	63.035	88
XS2	52	44.419	65
XS3	93	73.692	93
PAN	90	66.307	—

The forward and inverse transformation have been combined in one spread-sheet, as shown in Table 5. So each modification in the settings of the sensors can directly be translated into a modified algorithm for merging. The spreadsheet contains the calibration factors and the weighting factors per channel, the ultimate merging factors to be used and the result for one test pixel. With the calculated merging factors, the next three total equations can be derived for the SPOT images on 25/08/91. In the image processing system, the three equations for merging can be calculated per pixel, according to,

$$P_1^n = 0,915P_p + 0,428P_1 - 0,495P_2 \quad (12a)$$

$$P_2^n = 0,792P_p - 0,495P_1 + 0,572P_2 \quad (12b)$$

$$P_3^n = P_3 \quad (12c)$$

In Figure 4a, b and c the study area on the northwest coast of Walcheren is shown according to SPOT-PAN, SPOT-XS and SPOT-MRG (the result of merging the former two). The pixel values of the panchromatic channel are reproduced in various gray levels after histogram equalisation (Figure 4a). In Figure 4b and c, false color composites of the three multispectral channels of SPOT-XS and- MRG are reproduced after histogram equalisation. The Channels 3, 2 and 1 are in red, green and blue respectively.

Mapping Vegetation Structure in the Coastal Dune Area

The original and the enhanced multispectral image, SPOT-XS and-MRG, have been used in an unsupervised classification of the coastal dune (flowchart, Figure 2). The colored aerial photographs from 1988 and the supplementary maps (HEIDEMIJ, 1976; DUIN and KUST, 1991) have been used in combination to produce an overlay with the zonation of the vegetation structure classes. The 15 spectral classes have been translated into 14 thematic classes, varying from bare sand, grassland, shrubs and forest to open water (Figure 5 and Table 6).

Based on the aerial photograph interpretation 29 training sets have been selected interactively in the multispectral images. These training data have been used in the supervised classification of the natural vegetation in De Manteling/Oranjezon. The resulting 29 classes from two Maximum Likelihood-classifications, based on SPOT-MRG and-XS, have been combined into the desired 14 classes (table 6).

$$\begin{pmatrix} I_1 \\ I_2 \\ I_3 \end{pmatrix} = \begin{pmatrix} c_1 & c_2 & c_3 \\ -c_2 & c_1 & 0 \\ -c_1^2c_3 & -c_1c_2c_3 & c_1 \end{pmatrix} \begin{pmatrix} P_1 \\ P_2 \\ P_3 \end{pmatrix} \quad (9)$$

The third multispectral channel doesn't take part in the transformation and thus from equations (3) and (7b) follows: h₃ = 0 and c₃ = 0. This simplifies the matrix of the weighting factors considerably,

$$\begin{pmatrix} I_1 \\ I_2 \\ I_3 \end{pmatrix} = \begin{pmatrix} c_1 & c_2 & 0 \\ -c_2 & c_1 & 0 \\ 0 & 0 & c_1 \end{pmatrix} \begin{pmatrix} P_1 \\ P_2 \\ P_3 \end{pmatrix} \quad (10)$$

After replacing the simulated intensity (I_i) by the pixel value of the panchromatic channel (P_p), the inverse transformation into the new pixel values (P_iⁿ) looks as follows,

$$\begin{pmatrix} P_1^n \\ P_2^n \\ P_3^n \end{pmatrix} = \frac{1}{c_1^2 + c_2^2} \begin{pmatrix} c_1 & -c_2 & 0 \\ c_2 & c_1 & 0 \\ 0 & 0 & \frac{c_1^2 + c_2^2}{c_1} \end{pmatrix} \begin{pmatrix} P_p \\ I_2 \\ I_3 \end{pmatrix} \quad (11)$$



Figure 4. Northwest coast of Walcheren with dune area De Manteling/Oranjezon, SPOT 25/08/91. Original data Copyright (©) CNES 1991. a. Panchromatic data, SPOT-PAN (in gray levels). b. False color composite multispectral data, SPOT-XS. c. False color composite of merged multispectral and panchromatic data using Radiometric method, SPOT-MRG.

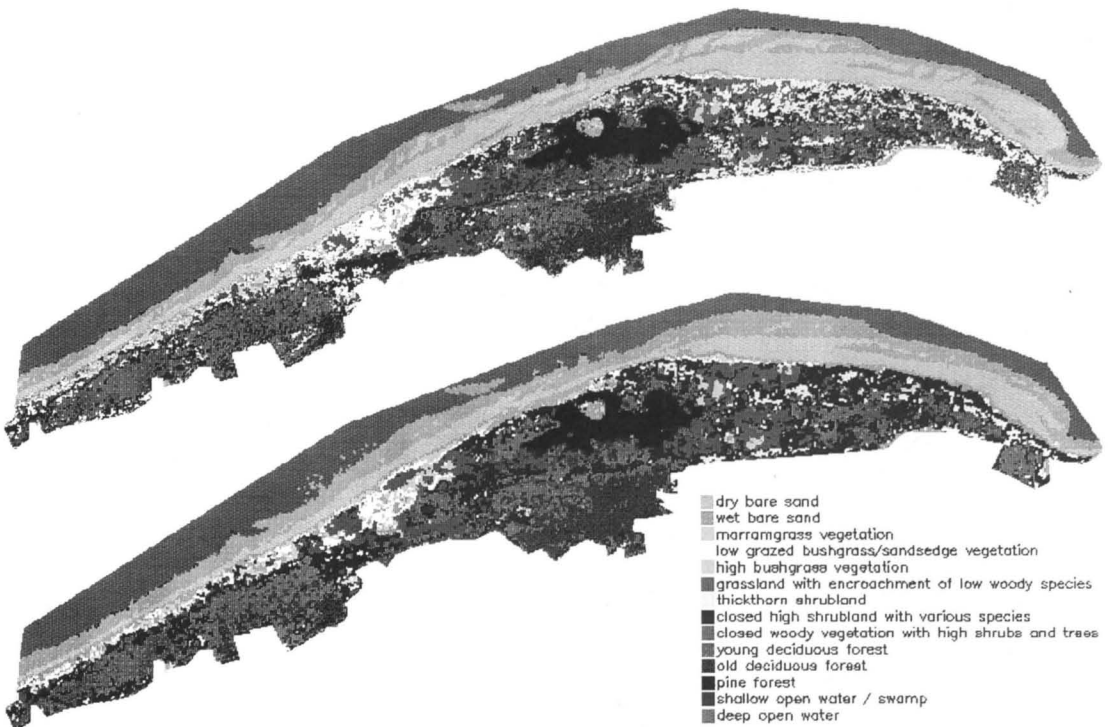


Figure 5. Vegetation structure map of coastal dune area De Manteling/Oranjezon, situation 25/08/91. a. Classification result based on merged multispectral and panchromatic data. b. Classification result based on multispectral data.

As a post-processing technique, thresholding has been applied to the class of marramgrass vegetation, based on probabilities from the supervised classification. Marramgrass, which is important for preservation of the sea wall and not likely to be found elsewhere, was initially overestimated in both classifications. From comparing both maps with the aerial photographs, it has been concluded that only the marramgrass pixels with probability, $p > 80\%$ were correctly classified. The remaining marramgrass pixels ($p < 80\%$) were re-coded to wet bare sand.

In Figure 5 the vegetation structure maps of De Manteling/Oranjezon are shown twice, based on SPOT-MRG (a) and -XS (b) respectively. The total coverage by vegetation in the dune area of De Manteling/Oranjezon is shown in Table 6. Accuracy and reliability of both maps have been tested by: (1) random comparison of the actual vegetation structure in the field with the classification results and (2) evaluation of the results based on SPOT-MRG and -XS for the total dune area using

a confusion matrix (Table 7). The expected surplus value of merging SPOT-PAN and -XS according to the Radiometric Method and its use in a supervised classification of natural vegetation is demonstrated under "Interpretation of results".

Mapping Spatial Distribution of Mean Annual Evapotranspiration in the Recharge Area

The evapotranspiration (ET) in Oranjezon can be calculated as the sum of evaporation (from interception water and soil water) and transpiration (water use by vegetation). Both processes are difficult to quantify in a heterogeneous dune area. Actual evapotranspiration in an average year is influenced by climatic conditions, type of vegetation cover, soil physical characteristics, topography, and, related to this, the depth of the groundwater table. However, from results of empirical research on water balances of the lysimeters near Castricum, situated in the northern dune district of the Netherlands (WIND, 1960; RIJTEMA

Table 6. Absolute and relative area covered by 14 types of vegetation structure in SPOT-MRG and SPOT-XS. De Manteling/Oranjezon 25/08/91

Vegetation Structure	Class Nr.	Area in SPOT-MRG		Area in SPOT-XS	
	DN	ha	%	ha	%
Dry bare sand	1	144.73	13.07	94.19	8.51
Wet bare sand	2	121.05	10.93	172.270	15.56
Marramgrass vegetation	3	7.55	0.68	11.59	1.05
Low grazed bushgrass	4	28.90	2.61	22.81	2.06
High bushgrass	5	20.46	1.58	22.93	2.07
Grassland & woody species	6	136.63	12.34	114.90	10.38
Thickthorn shrubland	7	74.32	6.71	21.52	1.94
Closed high shrubland	8	141.26	17.76	198.99	17.97
High shrubs and trees	9	30.39	2.74	22.02	1.99
Young deciduous forest	10	93.91	8.48	109.65	9.90
Old deciduous forest	11	57.71	5.21	67.57	6.10
Pine forest	12	33.21	3.00	36.39	3.29
Shallow open water/swamp	13	5.84	0.53	2.67	0.24
Deep open water	14	211.47	19.10	209.93	18.96
De Manteling/Oranjezon		1,107.43	100.00	1,107.43	100.00

and RYHINER, 1968; STUYFZAND, 1986, 1993), and from hydrological studies in the coastal dunes of the south-western delta of the Netherlands (BAKKER, 1981; PWS, 1988; IWACO, 1987) approximate annual ET-values per vegetation type could be deduced. Normal precipitation is based on measurements in Oranjezon during the period 1976–1985: $P=768$ mm/y. In view of the fact that the variation in ET-values that were found in the literature is large and the lysimeter measurements provide only indicative values for the different growing stages of spontaneous dune vegetation, a distinction has been made between two simplified situations with normal and above normal evapotranspiration. The normal situation and the above normal situation account for the uncertainty in mean annual evapotranspiration of dune grasslands and shrublands, as a result of dry or wet conditions at the site. Table 8 shows per vegetation structure type: normal precipitation (P in mm/y), annual evapotranspiration (ET in mm/y) and net precipitation ($P_n = P - ET$ in mm/y and m^3/y).

From the most reliable vegetation structure map (SPOT-MRG), the groundwater recharge area has been delineated. Within the area, corresponding ET-values have been attached to each pixel ($10 \cdot 10m^2$) of a particular vegetation structure class. Figure 6 illustrates a generalised version of the resulting ET-maps of Oranjezon in the normal and the above normal situation (a and b respectively). Six ET-classes with $200 < ET < 600$ mm/year are reproduced in colors, varying from red towards blue.

In coastal dunes in The Netherlands, the natural groundwater recharge practically equals the net precipitation since surface runoff and capillary rise are limited, due to the sandy soils and the low intensity rainfall typical of the region. So the spatial distributions of evapotranspiration, net precipitation and the natural groundwater recharge in Oranjezon can be assumed identical.

INTERPRETATION OF RESULTS

Panchromatic Multispectral and Merged Imagery

From a visual interpretation of the SPOT images (Figure 4a, b and c), it follows that the panchromatic image (SPOT-PAN) is much more fine-grained than the multispectral image (SPOT-XS). The sharp black and white picture itself has no value for vegetation mapping. In the multispectral image, a reasonable distinction can be made between various vegetation structures despite the absence of a band in the middle infrared. Figure 4c illustrates the better spatial and spectral resolution in the combination of the panchromatic and the multispectral image (SPOT-MRG). In SPOT-MRG, the most important landscape-elements can be distinguished: along the coast line deep and shallow open water and wet and dry sand; in and along the dune belt the pine forest, young and old deciduous forest, shrublands, grasslands and line shaped elements such as the two canals in east-west direction; and in the adjacent polders, the agricultural plots with various crops, and line shaped elements such as afforestation, verges and roads between the plots.

Table 7. Confusion matrix with areas of vegetation structure maps based on merged multispectral and panchromatic data (SPOT-MRG) and multispectral data (SPOT-XS). Coastal dune area De Manteling/Orajezon, 25/08/91. Corresponding classes are on the diagonal (in bold).

SPOT-XS	SPOT-MRG													
	Dry bare sand	Wet bare sand	Marram-grass vegetation	Low bushesandsedge	High bushesandsedge	Grassland & woody species	Thick-thorn shrubland	Closed high shrubland & var. species	Woody veg. high shrubs & trees	Young deciduous forest	Old deciduous forest	Pine forest	Shallow open water	Deep open water
Dry bare sand	62.4%	3.1%	0.4%	—	0.1%	—	—	—	—	—	—	—	—	—
Wet bare sand	90.3	36.5%	86.4%	4.2%	14.1%	0.8%	2.3%	0.6%	0.1%	0.2%	0.1%	0.2%	50.2%	1.0%
Marramgrass	52.9	104.6	1.7	1.2	2.9	1.1	1.7	0.9	—	0.2	0.1	0.1	2.9	—
Low bushesandsedge	0.8%	3.3%	62.7%	1.9%	5.5%	—	—	—	—	—	—	—	—	—
High bushesandsedge	1.1	4.0	4.7	0.6	1.1	—	—	—	—	—	—	—	—	—
Grassland & woody species	0.2%	2.3%	9.1%	39.3%	19.1%	1.7%	1.6%	0.2%	—	—	—	—	—	—
Thicketthorn shrubland	0.3	2.8	0.7	11.3	3.9	2.3	1.2	0.3	—	—	—	—	—	—
Closed high shrubland & var. species	—	0.7%	4.8%	20.0%	48.9%	4.0%	—	0.3%	—	—	—	—	—	—
Woody veg. high shrubs & trees	—	0.9	0.4	5.8	10.0	5.5	—	0.4	—	—	—	—	—	—
Young deciduous forest	—	0.2%	—	25.6%	1.1%	63.8%	5.5%	10.0%	—	1.3%	0.8%	—	—	—
Old deciduous forest	—	0.2	—	7.4	0.2	87.1	4.1	14.1	—	1.3	0.5	—	—	—
Pine forest	—	—	—	0.1%	—	—	21.7%	3.5%	0.9%	0.1%	—	—	—	—
Shallow open water	—	—	—	—	—	—	16.1	5.0	0.3	0.1	—	—	—	—
Deep open water	0.1%	2.1%	0.1%	9.0%	9.7%	26.3%	62.1%	65.3%	26.0%	8.0%	3.7%	0.2%	—	—
	—	2.5	—	2.6	2.0	35.9	46.1	92.7	7.9	7.5	2.1	0.1	—	—
	—	0.1%	—	—	1.5%	0.7%	3.6%	1.5%	40.7%	0.9%	4.7%	0.1%	—	—
	—	0.1	—	—	0.3	0.9	2.7	2.1	12.4	0.8	2.7	—	—	—
	—	0.1	—	—	—	1.7%	2.6%	16.5%	4.0%	82.1%	6.3%	—	—	—
	—	—	—	—	—	2.3	2.0	23.3	1.2	77.1	3.6	—	—	—
	—	—	—	—	—	1.1%	0.6%	0.9%	28.2%	7.5%	84.5%	—	—	—
	—	—	—	—	—	1.5	0.4	1.2	8.6	7.0	48.8	—	—	—
	—	—	—	—	0.1%	—	—	1.3%	—	—	99.5%	14.7%	—	0.1%
	—	—	—	—	—	—	—	1.8	—	—	33.0	0.9	—	0.2
	—	—	—	—	—	—	—	—	—	—	31.9%	1.9	—	0.1%
	—	—	—	—	—	—	—	—	—	—	—	3.3%	—	0.2
	—	—	—	—	—	—	—	—	—	—	—	—	98.9%	—
	—	—	—	—	—	—	—	—	—	—	—	—	—	209.2

Table 8. Some terms of the water balance per vegetation structure of groundwater recharge area Oranjezon, situation 1991.

Vegetation structure	Class	Area		P mm/yr	ET _{ref} [mm/yr]		P-ET [mm/yr]		P-ET [m ³ /yr]		
		DN	ha		%	Above		Above		Normal	Above Norm.
						Normal	Norm.	Normal	Norm.		
Dry bare sand	1	12.51	2.83	768	200	200	568	568	71,057	71,057	
Wet bare sand	2	28.45	6.43	768	300	300	468	468	133,146	133,146	
Marramgrass vegetation	3	5.94	1.34	768	300	300	468	468	27,799	27,799	
Low grazed bushgrass	4	21.69	4.90	768	350	400	418	368	90,664	79,819	
High bushgrass	5	13.91	3.14	768	350	400	418	368	58,144	51,189	
Grassland and woody species	6	91.78	20.75	768	380	430	388	338	356,106	310,216	
Thickethorn shrubland	7	14.66	3.31	768	380	450	388	318	56,881	46,619	
Closed high shrubland	8	133.24	30.12	768	380	450	388	318	516,971	423,703	
High shrubs and trees	9	9.01	2.04	768	400	480	368	288	33,157	25,949	
Young deciduous forest	10	49.80	11.26	768	450	500	318	268	158,364	133,464	
Old deciduous forest	11	20.64	4.67	768	550	550	218	218	44,995	44,995	
Pine forest	12	35.95	8.13	768	600	600	168	168	60,396	60,396	
Shallow open water/swamp	13	0.58	0.13	768	650	650	118	118	684	684	
Moreas	14	2.07	0.47	768	650	650	118	118	2,443	2,443	
Agricultural crops	15	2.14	0.48	768	350	400	418	368	8,945	7,875	
Recharge area Oranjezon		442.37	100.00						1,619,753	1,419,355	

Vegetation Structure Maps

In the vegetation structure maps based on SPOT-XS and SPOT-MRG (Figure 5a and b), the above mentioned characteristics can be found again. Following from the procedure, it can be assumed that differences in accuracy between both classifications are exclusively due to the extra information from the panchromatic channel and the related spatial resolution. When both vegetation structure maps are depicted at scale 1:10,000, it can clearly be seen that four identical grid cells in SPOT-MRG (10·10m²) form one original grid cell in SPOT-XS (20·20m²). However, for a substantial number of grid cells in SPOT-MRG (10·10m²), the extra information from the panchromatic channel resulted in a different vegetation type for at least one out of the four grid cells (10·10m²) that formed the original grid cell in SPOT-XS. So merging SPOT-XS and-PAN can be used to enhance spatial resolution, to improve rectification accuracies and to depict greater cartographic detail in both the resulting image and in the result of a supervised classification.

Besides the improved accuracy of the classification by merging SPOT-PAN and- XS, its reliability also improved. Both maps will be discussed for each vegetation class. With a confusion matrix for the total dune area (Table 7), the pure classification results based on SPOT-MRG (Figure 5a) and SPOT-XS (Figure 5b) are compared. The confusion matrix should be interpreted here dif-

ferent from what is normally done when evaluating classification results, using ground-truth. Since the aim is to signalize differences instead of resemblances between the two maps, especially low values on the diagonal are of interest. The related confusion in SPOT-XS indicates a potential surplus value of merging. For those classes with correspondence of the classification results higher than 80%, merging SPOT-XS and-PAN hardly improves the reliability of the vegetation map.

In SPOT-MRG dry and wet sand classes are found along the shore. This results in a larger area of dry sand along the accumulating coast in the north-east than in SPOT-XS (Table 6). The distinction between the dune slacks and the grazed grasslands in the west is also clear (the latter are yellow in Figure 5a). In SPOT-MRG two separate parts of a dune slack under construction and the small king fern dune slack, 100 meters north of the former, have been classified correctly. In SPOT-XS the transitions from wet to dry sand and from the bare sand to the grazed low bushgrass/sandsedge vegetation are less sharp (Table 7; dry sand vs. wet sand). A clear distinction between humic sand in the dune slacks and bare sand along the coast could not be made.

SPOT-MRG yields, compared to the fieldmap, a clear and reliable distinction between low bushgrass/sandsedge vegetation and high bushgrass vegetation. The former exists for 100% of grazed or cut grassland, the latter for 75% to 100% of

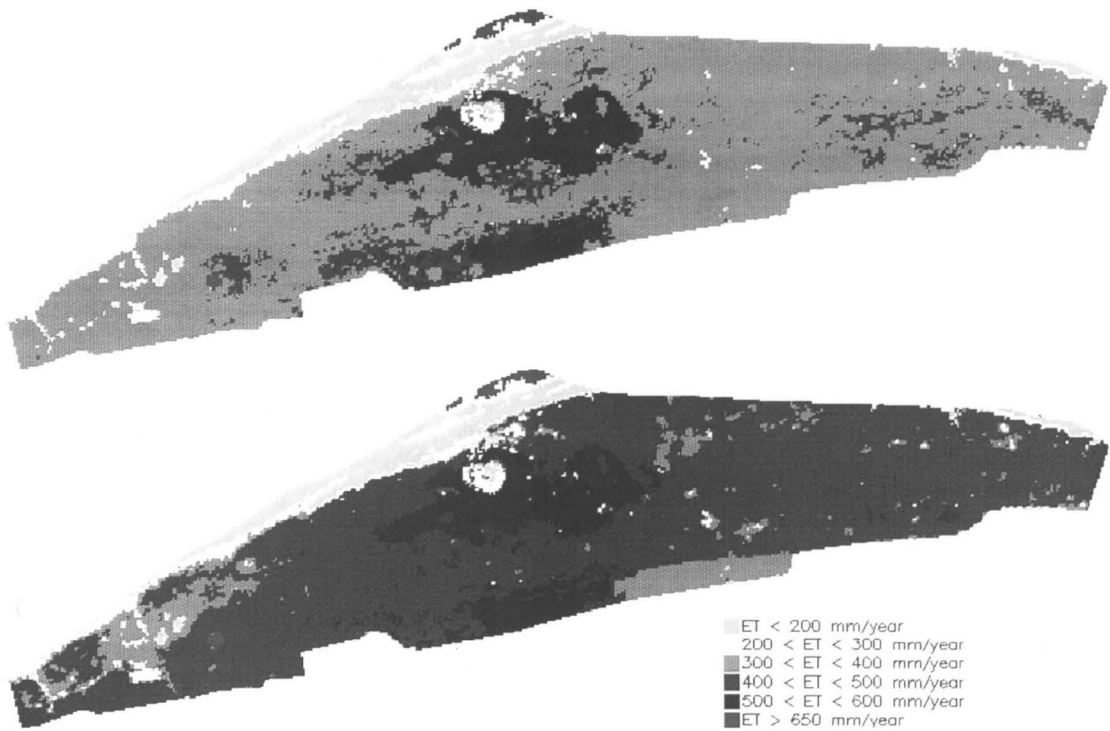


Figure 6. Evapotranspiration map of groundwater recharge area Oranjezon in 1991, based on merged multispectral and panchromatic data. ET-values in 6 classes [mm/y]. a. Normal evapotranspiration. b. Above normal evapotranspiration.

grassland dominated by high bushgrass. The grasslands in SPOT-XS do not match the reference map that accurately. High bushgrass vegetation is somewhat overestimated here.

The initial excessive occurrence of marramgrass in both classifications is directly related to the large bare sand area in which marramgrass was planted in rows. At the selection of the training data the spectral characteristics of both the vegetation and the (apparent moist) sand were defined. This is inevitable. By applying thresholding as a post-processing technique, practically all sand pixels have been removed from this class. Besides the fact that selecting acceptable training data is easier in SPOT-MRG than in SPOT-XS, the distinction between marramgrass and moist sand is better in SPOT-MRG (Tables 6 and 7).

The dunes of De Manteling/Oranjezon are according to SPOT-MRG for a substantial part covered by grassland, with encroachment of low woody species (Table 6; 12%). Within this class grass-

land and shrubland/low trees, cover 50% of the surface. The shrubland shows a large variation in species such as, thickthorn, elder, dog-rose, hawthorn and blackberry. The low trees are birch, prunus, oak and maple. About 13% is covered by closed high shrubland with various species. From Table 6 it follows that SPOT-XS yields considerably less grassland (10%) and more closed high shrubland with various species (18%) than SPOT-MRG. The last difference can be explained with Figure 5 and Table 7. Especially in the east of the groundwater recharge area, SPOT-MRG is distinguished by the separate class thickthorn shrubland (75% to 100% thickthorn). In SPOT-XS, 62% of the thickthorns go to closed high shrubland with various species. Thus, here merging improves supervised classification results significantly.

The separation of the classes closed high shrubland with various species and closed woody vegetation with high shrubs and trees is due to the

frequent occurrence of trees in the latter. High woody vegetation with high shrubs and trees is mapped on a very small scale in both images (Table 6; 2% and 3% respectively). However, differences between SPOT-MRG and SPOT-XS are large (Table 7). For only 41% of the area where SPOT-MRG classifies closed woody vegetation with high shrubs and trees, SPOT-XS does the same. Confusion with closed high shrublands and deciduous forest is probably larger in SPOT-XS than in SPOT-MRG (Table 7). On the basis of the aerial photographs, this distinction could not clearly be made. Particularly in the forested area De Manteling, SPOT-MRG accurately classifies high shrubs and young and old deciduous forest (Figure 5).

From Tables 6 and 7, it follows that merging has no surplus value for relatively homogeneous classes in a supervised classification. The results of SPOT-MRG and SPOT-XS correspond for young and old deciduous forest, pine forest and deep open water at 82%, 85%, 100% and 99% respectively. Young deciduous forest is defined here as low spontaneous trees, particularly within the dune area, such as birch, prunus and oak. Old deciduous forest is planted and can be found in particular on the inland side of the dune belt and on the adjacent estates. Known homogeneous plots with poplar for production could not be classified separately.

Merging can be very useful for classification of small wet landscape-elements. Shallow open water and swamps are mapped on a very small scale in both images (Table 6; < 0.53%), but Figure 5 and Table 7 illustrate the surplus value of merging. Some small wet landscape-elements that can be found in the groundwater recharge area are: a decoy, southeast of the grazed grasslands, a sand pit with a small pool, surrounded by pine forest, and narrow open canals in the east-west direction. Along the coast line, shallow open water is distinguished from wet sand and deep North Sea water. For only 32% of the area, SPOT-MRG and SPOT-XS both classify as shallow open water/swamp (Table 7). In SPOT-MRG, 5.84 ha is classified as shallow open water/swamp, against 2.67 ha in SPOT-XS (Table 6). The double area in SPOT-MRG is exclusively due to the extra information from the panchromatic channel. In SPOT-XS shallow open water and wet bare sand are very hard to distinguish, in particular along the coastline (Table 7; 50,2%). Spectrally seen, this is not unexpected. The open canals are too

small to be detected with the 10 m resolution of SPOT-MRG. Only where the canal cuts through the pine forest in the northwest is shallow open water classified. In the main part of Oranjezon, the canals can be recognized by the strips of grassland and the shrubs along them (Figures 4 and 5).

Evapotranspiration Maps

The ET-maps in Figure 6a and b illustrate the detailed spatial distribution of the calculated factors of the waterbalance in Table 8. The spatial resolution of both ET-maps is directly related to the resolution of the original images and the vegetation structure map (SPOT-MRG).

Differences in the ET-maps of Oranjezon for normal and above normal evapotranspiration can be explained in particular by the highly variable evapotranspiration of grassland, shrubland and young deciduous forest. Variable evapotranspiration causes differences in net precipitation, or the natural recharge of the groundwater. For the total groundwater recharge area, the difference amounts to over 2.00 10⁶ m³/year (Table 8).

The large spatial variation in annual ET-values and natural groundwater recharge (Figure 6) demonstrates that using average ET-values for selected compartments of the steady state groundwater model of the dune area (IWACO, 1987) will cause considerable inaccuracy. With this simple empirical approach, a more accurate value for net precipitation can be attached to each knot of the finite elements network of the groundwater model of Oranjezon.

The reader should be aware of the fact that the mapped evapotranspiration and net precipitation are not intended to be observations for any specific time but are two suggested first cut estimates which allow approximating groundwater recharge.

At present the effect of nature regeneration on vegetation structure and waterbalance of the groundwater recharge area is being studied. For the calculation of the total amount of water that will be available for vegetation or groundwater extraction after the recent reconstruction of the dune slacks, the same approach is being followed using a transient flow model and ET-referential values on a monthly basis (HOBMA *et al.*, 1995).

CONCLUSION AND OUTLOOK

With the described method for merging multispectral and panchromatic satellite imagery, it

has been demonstrated how a recent vegetation structure map of a coastal dune area can be produced, using SPOT-XS and-PAN, old reference maps and a limited amount of field work.

In addition to the improved visual interpretation of the image, merging SPOT-XS and-PAN by the Radiometric Method yields clearly better results in a supervised classification of natural vegetation than the usual classification, exclusively based on SPOT-XS. In the resulting image from merging and the derived thematic maps, the better spatial and spectral resolution of the panchromatic and the multispectral image respectively are combined. In particular when the landscape is fine-grained, the increased accuracy and reliability of the classification results balance the heavily increased amounts of data and the extra computing time required.

With the presented summary of the possible calibration coefficients for SPOT1 and-2, the actual instrument setting during observation and the test case for implementation of the algorithm in a spreadsheet, merging SPOT-XS and-PAN with the Radiometric Method, can be operationally used in every image processing system. When absolute calibration values per channel are available, the Radiometric Method for merging can be applied on every combination of multispectral and panchromatic imagery, without a limit to the maximum number of channels. Compared to other merging algorithms, like Intensity Hue Saturation (IHS), Spherical Coordinate or the Statistical method (PELLEMANS *et al.*, 1993), computing time will remain acceptable for operational use.

Since the Radiometric Method preserves absolute pixel values in the merging process, post-processing algorithms, like vegetation indices, become more useful compared to the usual application on non-calibrated multispectral images.

In the coastal dune area De Manteling/Oranjezon 14 types of vegetation structure could be clearly distinguished in a supervised classification of merged multispectral and panchromatic imagery. Except for young and old deciduous forest, pine forest and deep open water, it has been demonstrated that merging with the Radiometric Method improves classification accuracy and reliability of the vegetation structure map.

The large spatial variation in annual evapotranspiration (ET) in the heterogeneous coastal dune demonstrates that using average ET-values for a few compartments of the steady state geohydrological model of Oranjezon will cause con-

siderable inaccuracy. With the described empirical approach, values of net precipitation can be attached to the finite elements network of the geohydrological model at increased spatial resolution. By optimising other boundary conditions, the suitability of geohydrological models for ecohydrological interpretation will be increased.

It is common knowledge that the better spectral resolution of Landsat-4 and-5 yields better results in a supervised classification of natural vegetation and landuse than the better spatial resolution of SPOT1 and-2 (in multispectral mode). Promising developments with respect to future imagery from these platforms makes combined use of multispectral and panchromatic data an interesting topic, because:

- (1) In 1997 SPOT4 will provide both multispectral (including middle infrared) and panchromatic data at a spatial resolution of 20 m and 10 m respectively.
- (2) The first dual resolution imagery of Landsat-7 will provide both multispectral (including middle infrared) and panchromatic data at a spatial resolution of 30 m and 15 m respectively.
- (3) SPOT-5 will provide both multispectral and panchromatic data at a spatial resolution of 10 m and 5 m respectively!

The last option is a dream for the future; but with the new generation of dual resolution instruments, the application of satellite remote sensing for mapping natural vegetation and landscape elements at a sub-regional scale will be greatly improved. For those scientists seeking to maximize the amount of information that can be extracted from available satellite image data, the good times have just begun.

ACKNOWLEDGEMENTS

I am indebted to Adriaan van de Griend and two anonymous reviewers for their valuable comments and suggestions. I also thank Alfred Pellemans and Henk Kloosterman at the Surveying Department of Rijkswaterstaat for helpful discussions in the preparation of this paper. Some characteristics of SPOT4 and Landsat-6 were kindly provided by Frank Wouters and Leen van der Meer of the National Aerospace Laboratory (NLR). Financial support from the Cornelis Lely Stichting of Rijkswaterstaat and the Netherlands

Remote Sensing Board (BCRS) is gratefully acknowledged.

LITERATURE CITED

- BAKKER, T.W.M., 1981. Dutch Coastal Dunes; Geohydrology. Report ISBN 90 0758 8/Ph.D. Thesis, Agricultural University Wageningen, pp 189.
- CARPER, W.J.; LILLESAND, T.M., and KIEFER, R.W., 1990. The Use of Intensity-Hue-Saturation transformations for merging SPOT panchromatic and multispectral data. *Photogrammetric Engineering and Remote Sensing*, 56(4), 459-467.
- CHAVEZ, P.S.; SIDES, S.C., and ANDERSON, J.A., 1991. Comparison of three different methods to merge multi-resolution and multispectral data: Landsat TM and SPOT Panchromatic. *Photogrammetric Engineering and Remote Sensing*, 57(3), 295-303.
- DUIN and KUST, 1991. Monitoring of measures against acidification in Oranjezon. Report *First Object, Phase 1: Fieldwork 1991* (in Dutch).
- HEIDEMIJ, 1976. Management plan Oranjezon. Report *Heidemij Consultants*. Hoofddorp (in Dutch).
- HOBMA, T.W., 1991. Application of remote sensing and hydrological models in ecohydrological research in two lowland brook valleys in the Province of Drenthe. The Winand Staring Centre DLO en Agricultural University of Wageningen, *Internal Report nr. 218*. Wageningen (in Dutch).
- HOBMA, T.W., DE HAMER, A., and BAKKER, A., 1994. Regeneration of wet dune slacks in the south-western delta of the Netherlands: HYFA a useful tool to predict future evolution. *Proceedings: Second International Conference on Groundwater Ecology* (Atlanta Hilton & Towers, Atlanta, Georgia, March 27-30, 1994).
- HOBMA, T.W., JANSSEN, L.F., and BOTTELIER, R.C., 1995. Remote sensing and GIS supported groundwater modelling of a coastal dune in the south-western delta of the Netherlands. *EARSel-journal "Advances in Remote Sensing"* (accepted): *Proceedings Workshop on Remote Sensing and GIS for Coastal Zone Management*. Delft, The Netherlands, 24-26 October 1994.
- IWACO, 1987. Geohydrological research Oranjezon, Phase 1: Inventarisatie Geohydrology. Report *IWACO Consultants*. Boxtel (in Dutch).
- MUNECHIKA; WARNICK; SALVAGGIO and SCHOTT, 1993. Resolution enhancement of multispectral image data to improve classification accuracy. *Photogrammetric Engineering and Remote Sensing*, 54(1), 67-72.
- NATIONAL AEROSPACE LABORATORY (NLR), 1993. Parameter summaries of Landsat-6, Enhanced Thematic Mapper and SPOT4.
- PELLEMANS, A.H.J.M.; JORDANS, R.W.L., and ALLEWIJN, R., 1993. Merging multispectral and panchromatic SPOT images with respect to the radiometric properties of the sensor. *Photogrammetric Engineering and Remote Sensing*, 1, 81-87.
- PRICE, J.C., 1987a. Calibration of Satellite Radiometers and the Comparison of Vegetation Indices. *Remote Sensing of Environment*, 21, 15-27.
- PRICE, J.C., 1987b. Combining Panchromatic and Multispectral Imagery from Dual Resolution Instruments. *Remote Sensing of Environment*, 21, 119-128.
- PROVINCIALE WATERSTAAT ZEELAND, 1988. Groundwater plan Schouwen: Plan concept and Explanation. *Public Document Province of Zeeland*. Middelburg (in Dutch).
- SPOT IMAGE, 1988. *User's Handbook, Vol. 1+2: Reference Manual and Handbook*.
- SPOT IMAGE, 1992. *SPOT Newsletter*, 18, 1.
- STUYFZAND, P.J., 1986. Waterbalances and residence times in four, different overgrown lysimeters near Castricum. Report *KIWA*. Rijswijk.
- STUYFZAND, P.J., 1993. Hydrology and hydrochemistry of the coastal dune area of the Western Netherlands. Report *KIWA I11 Nieuwegein/Ph.D. Thesis*, Free University Amsterdam.
- WELCH, R., and EHLERS, M., 1987. Merging Multiresolution SPOT HRV and Landsat TM Data. *Photogrammetric Engineering and Remote Sensing*, 53(3), 301-303.
- WIND, R., 1960. The lysimeters in the Netherlands. In: *TNO Committee on Hydrological Research, Proceedings and Information* (3), pp. 165-228.